Progress in Oceanography 128 (2014) 74–87

Contents lists available at ScienceDirect

Progress in Oceanography

journal homepage: www.elsevier.com/locate/pocean

Horizontal dispersion in shelf seas: High resolution modelling as an aid to sparse sampling

Nataliya Stashchuk [a,*], Vasiliy Vlasenko [a], Mark E. Inall [b], Dmitry Aleynik [b]

[a] School of Marine Science and Engineering, University of Plymouth, Drake Circus, Plymouth, PL4 8AA, UK
[b] Scottish Association for Marine Science, Scottish Marine Institute Oban, Argyll, PA37 1QAT, UK

ARTICLE INFO

Article history:
Received 22 November 2013
Received in revised form 24 June 2014
Accepted 16 August 2014
Available online 28 August 2014

ABSTRACT

The ability of a hydrodynamic model to reproduce the results of a dye release experiment conducted in a wide shelf sea environment was investigated with the help of the Massachusetts Institute of Technology general circulation model (MITgcm). In the field experiment a fluorescent tracer, Rhodamine WT, was injected into the seasonal pycnocline, and its evolution was tracked for two days using a towed undulating vehicle equipped with a fluorometer and a CTD. With a 50 m horizontal resolution grid, and with three different forcings initialized in the model (viz: tides, stationary current, and wind stress on the free surface), it was possible to replicate the dye patch evolution quite accurately. The mechanisms responsible for the enhancement of horizontal dispersion were investigated on the basis of the model results. It was found that enhancement of the dye dispersion was controlled by vertically sheared currents that, in combination with vertical diapycnal mixing, led to a substantial increase in the "effective" horizontal mixing. The values of "effective" horizontal mixing found from the model runs were in good agreement with those obtained from in-situ data, and the probable degree to which the observational techniques undersampled the dye patch was revealed.

Introduction

Isolated underwater topographies are known as potential sources for mesoscale and finescale oceanic variability and are therefore of great importance to the local and regional ecology through enhanced mixing in the vertical and horizontal. Strong tidal currents and wind driven flows can enhance vertical mixing in the areas of underwater banks (Nash and Moum, 2001; Vlasenko et al., 2013). The Celtic Sea, with its wide shelf (~ 250 km), contains a number of such underwater features. One of them, Jones Bank (Fig. 1), located in the central part of the Celtic Sea shelf, was the study area for the 25-th cruise of the R/V *"James Cook"* (hereafter JC25). One of the goals of the field campaign was an investigation of the mixing processes that control horizontal dispersion and vertical eddy diffusion of a passive tracer released during JC25. Rhodamine WT, a fluorescent dye tracer, was injected into the seasonal pycnocline at the depth of the buoyancy frequency maximum (approximately 35 m). The methodological details of the experiment are reported in the paper by Inall et al. (2013).

Two dominant dynamical processes acting in the area of Jones Bank are the tides and wind driven motions. Both processes generate vertical shears in the background currents that can affect horizontal dispersion. Inall et al. (2013) performed an analysis of the spectrum of oceanic currents recorded at the mooring MS1 located at the top of the bank (see Fig. 1) and found that the temporal variability of the vertical shear of the horizontal currents within the thermocline was dominated by inertial oscillations at the time of observation. As a result, the main conclusion derived by Inall et al. (2013) was a recognition that the horizontal dispersion in the dye release experiment was remarkably enhanced by the vertical shear related to inertial oscillations (wind driven shear dispersion). The possibility of such a mechanism of intensification of horizontal mixing by vertical diapycnal exchange in low frequency ocsillating vertically sheared currents was pointed out by Young et al. (1982), but had not been witnessed in situ until the work of Inall et al. (2013).

It should be noted here, and borne in mind throughout this paper, that it is a challenging task to keep track of a sub-surface dye patch over many days using just ship-mounted equipment. Continuous, synoptic tracking can be done only by an aircraft that flies around the dye patch during several days conducting measurements remotely, which is an expensive procedure. An alternative and more commonly used methodology (Sundermeyer and

* Corresponding author.
E-mail address: nstashchuk@plymouth.ac.uk (N. Stashchuk).

http://dx.doi.org/10.1016/j.pocean.2014.08.007
0079-6611/

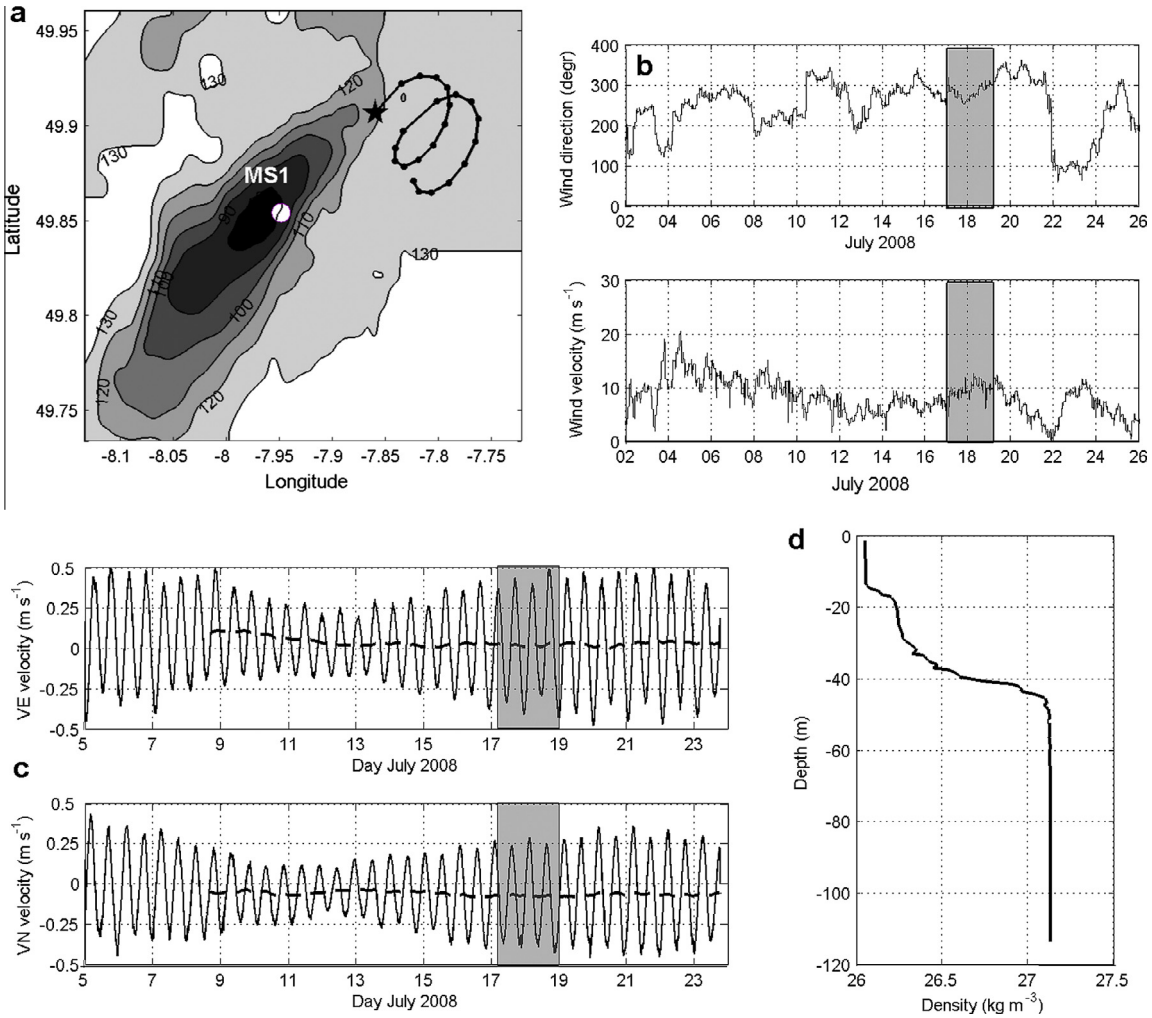

Fig. 1. (a) Bathymetry of Jones Bank, drifter track for the first 24 h after dye release (black dots and lines). Pentagram shows the position at the bank where dye and drifter were released. Position of the moorings MS1 is shown by closed white circle. (b) Wind direction and velocity during JC25. Rectangles correspond to dye release time interval. (c) Zonal and meridional vertically averaged velocities recorded at mooring MS1. Dashed lines show stationary currents. Rectangles correspond to dye release time interval. (d) CTD profile of density on the 17th of July 2008.

Ledwell, 2001) is to deploy an undulating device towed behind a moving vessel that can record the dye concentration in real time. Such an approach allows for the dye to be mapped along the ship's track over several days for relatively low cost, but it is still not good enough to give a complete picture of the tracer dispersion, in the sense that objective maps of the dye concentration have to be reconstructed from often sparse sampling of the real dye distribution. The absence of dye data beyond the tracks produces the gaps in observational data that is entirely expected in any real observational campaign. In many of these cases it is some kind of art to evaluate the characteristics of the mixing processes correctly using sparse data because of some unavoidable level of uncertainty. Such are the known limitations of dye release experiments.

The main goal of the present study was to simulate numerically the dye release experiment conducted near Jones Bank during JC25 and to compare the model-predicted dye fields with the in-situ data to answer the questions whether numerical modelling can firstly corroborate observational analyses and secondly provide a deeper insight into an understanding of the dye evolution. The paper is organized as follows. Section "JC25 experiment" discusses the details of the field experiment. Section "Numerical model" briefly outlines the model details. Section "Modelling of the dynamical processes" presents modelling results of the dynamical processes operating in the area under investigation and Section "Replication of the dye release experiment" describes modelling of the dye release. The paper ends with a discussion and some conclusions.

JC25 experiment

Moorings with thermistor chains and Acoustic Doppler Current Profilers (ADCP) were deployed at the beginning of the JC25 (Inall et al., 2013). For the dye release Rhodamine WT was chosen as a passive tracer due to its ability to be detectable for several days after release at a level sufficient for detection by a fluorometer (details can be found in Ledwell et al. (2004)). The fluorometer was mounted in a towed Scanfish vehicle which scanned the whole water column undulating from 5 m below the surface to a depth of 10 m above the bed. Scanfish cycled every 2 min giving an effective horizontal resolution of approximately 250 m.

Strong north-westerly winds were recorded at the beginning of July with wind speed over 15 m s^{-1} on 5-th July, Fig. 1b. After quite stormy conditions the wind speed dropped steadily by July 13-th, but the wind-induced circulation remained in the area and affected all dynamical processes including the dye dispersion. The ADCP signal recorded at the mooring MS1 revealed a background

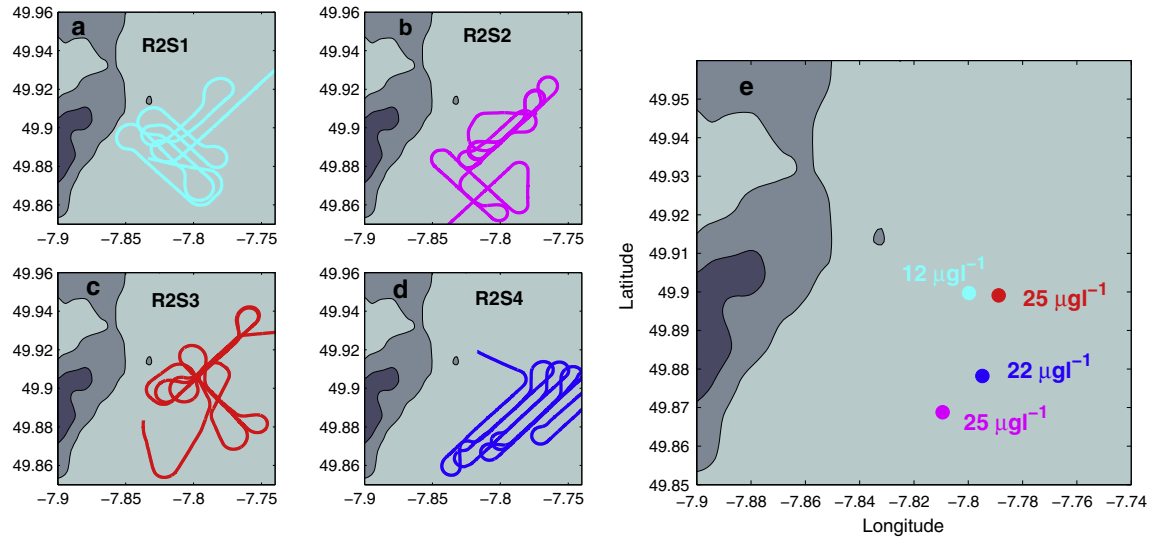

Fig. 2. (a), (b), (c) and (d) Four tracks of Scanfish surveys R2S1, R2S2, R2S3 and R2S4. (e) Closed circles with the colours that correspond to each survey show the positions where the largest concentrations of Rhodamine were found during each survey with corresponding values of the concentrations.

southward depth averaged current with velocity about 0.05 m s^{-1}, Fig. 1c.

The dye release was started on 17 July at 02:00 and the last survey of the Scanfish was finished on 18 July at 23:35, lasting approximately two days in total. During the experiment the westerly wind velocity was around 9 m s^{-1}, Fig. 1b. Rhodamine was injected into the pycnocline layer at the depth of the isopycnal σ_θ = 26.5 kg m^{-3} at the location shown in Fig. 1a by the black pentagram. The vertical position of the dye injection was slightly above the maximum density gradient which was located at a depth about 35 m, Fig. 1d. Spatial stratification in the dye-release region surrounding the Jones Bank was quite homogeneous: no strong horizontal frontal features were observed. In addition to the Rhodamine release, a 35-meter-drouged Lagrangian drifter was deployed in the area. Its position was recorded remotely every hour (for the drifter trajectory see Fig. 1a).

Four 5–6 h Scanfish/fluorometer surveys named as R2S1, R2S2, R2S3 and R2S4 were carried out. They started on the 5-th, 14-th, 28-th and 39-th hour after the dye release, Fig. 2a–e.

Numerical model

The Massachusetts Institute of Technology general circulation model (MITgcm) (Marshall et al., 1997) was used to simulate the dye release experiment. The barotropic tidal forcing was initialized in the model through extra periodical terms added to the right hand side (RHS) of the momentum balance equations. The original MITgcm code does not include tidal forcing directly. However, the model allows users to make modifications by introducing their own packages into the code as a "my-package" option. In our case a "tidal package" that adds the tidal potential in the RHS of the momentum balance equations was added the MITgcm code. Due to the short time interval of the numerical experiment (two days) that does not reveal significant neap-spring tidal variability we have restricted our analysis to a consideration of the dominant M2 semi-diurnal periodic potential function.

The amplitudes of the extra tidal terms were chosen in such a way as to generate realistic values for barotropic tidal currents that at the position of the mooring MS1 had an amplitide of approximately 0.45 m s^{-1}. Verification of the code for a homogeneous fluid was conducted by comparing the model output with the predictions of the global inverse tidal model, TPXO7.1, (Egbert and Erofeeva, 2002) and observational data. The two-dimensional structure of the tidal ellipses shown in Fig. 3a was reproduced by the modified code quite accurately. The parameters for the tidal forcing were chosen in such a way to replicate the direction and length of minor and major semi-axis of tidal ellipses. The details of the tidal currents recorded at mooring MS1 and their model counterparts are reported in our earlier paper (Vlasenko et al., 2013).

After setting the barotropic tidal forcing, the model was run with a stratified fluid. The profile for the background fluid stratification was taken directly from the CTD measurements from JC25, Fig. 1d. The model domain with the underwater bank is shown in Fig. 1a. It was approximated by a 595 × 491 model grid in the code with a horizontal resolution of 50 m in both zonal and meridional directions. In addition to the central part of the domain, 386 steps were added to the model grid at the northern, southern, western and eastern boundaries, transforming it into a 1383 × 1279 grid. In these extra lateral areas the grid resolution gradually changed from a 50 m spatial step in its central part to 50 km at the boundary. Such a telescopic increase of the horizontal steps towards the periphery eliminated the reflection of the waves from the model boundaries for at least 10 tidal cycles. The vertical grid step Δz was equal to 5 m in the upper surface 40 m layer and below it Δz was increased to 10 m.

The vertical turbulent closure for the coefficients of vertical viscosity ν and diffusivity κ was provided by the Richardson number dependent parameterization (Pacanowski and Philander, 1981):

$$\nu = \frac{\nu_0}{(1+\alpha \mathrm{Ri})^n} + \nu_b, \quad \kappa = \frac{\nu}{(1+\alpha \mathrm{Ri})} + \kappa_b.$$

Here Ri is the Richardson number, $\mathrm{Ri} = N^2(z)/(u_z^2 + v_z^2)$, and $N^2(z) = -g/\rho(\partial\rho/\partial z)$ is the buoyancy frequency (g is the acceleration due to gravity and ρ is the density), u and v are the components of horizontal velocity; $\nu_b = 10^{-5}$ m^2 s^{-1} and $\kappa_b = 10^{-5}$ m^2 s^{-1} are the background parameters, $\nu_0 = 1.5 \cdot 10^{-2}$ m^2 s^{-1}, $\alpha = 5$ and $n = 1$ are the adjustable parameters. Such a dependence increases ν and κ in the areas where the Richardson number is small which should parameterize the mixing processes induced by the shear instabilities and breaking internal waves. The horizontal viscosity A_h and diffusivity K_h were taken as constant, with a value of 0.5 m^2 s^{-1}. A full justification of this choice is discussed in the next section.

The Rhodamine was set in the model as a passive tracer using an extra transport equation:

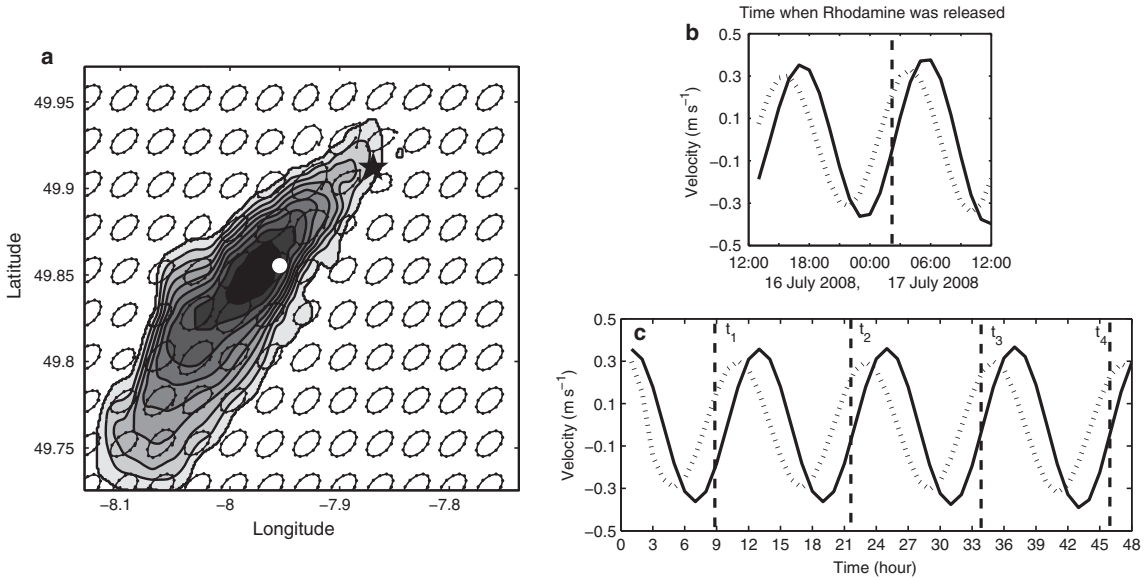

Fig. 3. (a) Tidal ellipses produced by MITgcm in homogeneous fluid. The position where drifter was released and mooring MS1 are shown by pentagram and closed circle, respectively. (b) Tidal velocities for the area of Jones Bank obtained from TPXO7.1. Vertical solid line shows the time when the Rhodanime was released. (c) Tidal velocities produced by MITgcm. Solid and dotted lines show eastward and northward velocities, respectively. Vertical dashed lines marked by t_1, t_2, t_3 and t_4 indicate start times of the numerical experiments with drifter releases.

$$\frac{\partial C}{\partial t} + u\frac{\partial C}{\partial x} + v\frac{\partial C}{\partial y} + w\frac{\partial C}{\partial z} = K_h\frac{\partial^2 C}{\partial x^2} + K_h\frac{\partial^2 C}{\partial y^2} + \kappa\frac{\partial^2 C}{\partial z^2}. \quad (1)$$

Here C is the concentration of the tracer, and (u, v) are the horizontal and (w) vertical velocity components. In the model runs the calculation of the transport equation for the passive tracer was started at the moment in time when the dye was injected. The initial field of C was zero everywhere except for one grid cell with coordinates 49.90615N and 7.859162W at a depth of 35 m, where its concentration was set to 1.

The concentration of the tracer changed due to diffusion and advection as the model was integrated forward in time. The centred second-order method which requires a second order time-stepping scheme (or quasi-second order Adams-Bashford scheme) to be stable are used in MITgcm for tracers by default. As a payment for higher accuracy such schemes normally introduce undesirable high frequency noise into the solution. In order to reduce the noise some scale-selective diffusion corrections should be employed. In the dye release experiment considered here with the initially sharp frontal interface of the tracer (and propagating fronts during the tidal stirring of the patch afterwards), the use of the flux limited schemes is essential. The second order flux limited scheme, set in MITgcm as scheme 77, was used here in modelling the Rhodamine evolution. It uses more numerical time than the basic centred second order scheme, but the reward is in its improved performance for the tracer modelling. Special code was written to calculate the position of the dye patch where the largest value of the tracer was located. The position of the maximal value of the tracer concentration at the depth of 35 m was treated as equivalent to the position of the drifter with the drogue depth of 35 m or as the maximal value of the Rhodamine concentration.

Modelling of the dynamical processes

A series of three numerical experiments were conducted with the following driving forces included into the model: (i) periodical tidal currents, (ii) steady-state flow, and (iii) wind stress. To determine their specific contribution, the forces were activated one by one in the model.

(i) It is important to start the drifter in the model exactly at the same tidal phase as in the field experiment. In the field the 35-meter-drogues drifter was released at 02:12 on July 17-th, 2008. Due to the periodicity the tidal phase at time $t_1 = 9$ h, $t_2 = 21.42$ h, $t_3 = 33.84$ h and $t_4 = 46.26$ h, Fig. 3c, is equal to tidal phase during release (shown by the vertical line in Fig. 3b). From a first glance it should not matter in which tidal cycle the tracer is released: as long as the process is periodical, the result should be the same. In reality the spin-up time of the model is always required to eliminate the influence of the initial conditions.

Fig. 4a shows that the drifter released 9 h after the beginning of the model run completed two tidal ellipses. However, the drifter that was released 12 h later completed just one tidal ellipse and then it was advected to the north after a receding loop, Fig. 4b. The drifters released 33 and 45 h after the start of model run propagated to the north with similar loops without ellipses in the beginning, Fig. 4c and d. Such a difference in the drifter motion between the last two and the first two cases testify to the presence of some sort of a current generated near the bank at the depth of drogue of Lagrangian drifter during the first two tidal cycles. By the end of the third tidal cycle the spin-up of the model is complete because all transitional processes are attenuated and the system came to a quasi-periodical state.

The spatial structure of the current at the depth of 35 m was found by integrating the model output over four tidal cycles Fig. 5a. The strongest part of current that flows in the north-east direction with maximum velocity up to 0.13 m s^{-1} is originated over the summit of the bank. The current at the depth of 35 m is different from the residual depth integrated clockwise rotated current (Huthnance, 1974; Loder, 1980; Beckmann, 1995; Kowalik and Marchenko, 2002).

(ii) It is clear that an extra background southward directed current should exist in the model to arrest the drifter to the east from the bank. In fact, such a current was present at mooring MS1 after filtering the ADCP time series with 25 h moving averaging window that removed the tidal harmonics. This revealed a southward stationary current with velocity 0.06 m s^{-1} on 17–19 July, shown by the black dashed lines in Fig. 1c, and was probably generated by the wind in the beginning of July.

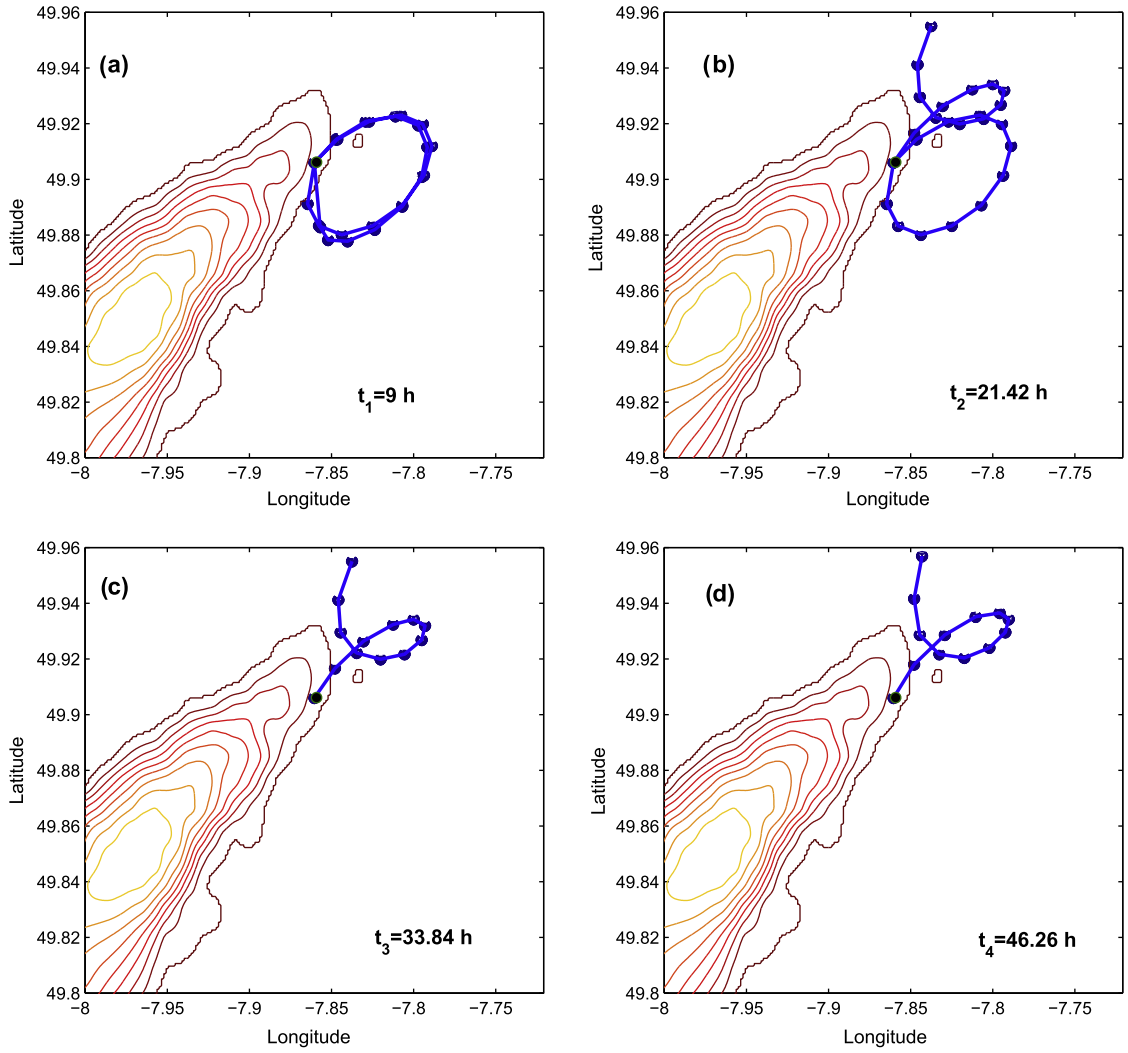

Fig. 4. Model spin-up: (a), (b), (c) and (d) depict two tidal periods tracks of the model drifter that was released 9, 21.42, 33.84 and 46.26 h after the beginning of the numerical experiment. The time interval between two neighbouring asterisks connected by line equals one hour.

In a similar manner to the tidal forcing, the stationary, 0.06 m s^{-1}, current was initialized in the model by extra terms that were added to the RHS of the momentum balance equations. Methodologically, the tidal forcing was activated in the code only after a stationary current was established in the model domain, and a new drifter trajectory was calculated for four tidal cycles, Fig. 5b. The absence of the along-bank jet that was generated due to the tides is obvious and the new drifter trajectory is shifted to the east of the bank. However, the drifter trajectory is still quite different from the real drifter 24-h track shown in Fig. 5d.

(iii) In fact, a north-west wind with velocity of about 9 m s^{-1} (see Fig. 1b) was blowing during the two days of the dye release and was able to modify the currents. The residual currents at the depth of 35 m generated by all three forcing terms, i.e. tides, currents, and wind are presented in Fig. 5c. The trajectory of the model drifter is closer to the real drifter route now, Fig. 5d, and thus the code was ready to simulate the evolution of the dye in as realistic manner as possible.

Replication of the dye release experiment

The dye patch injected into the pycnocline migrated permanently due to several dynamical processes. The tide was the most predictable process because the direction and strength of the tidal current can be estimated in advance. With such a conception the track of each Scanfish survey was recalculated in a reference frame moving with the observed tidal flow (Inall et al., 2013). If the latter was subtracted correctly, the dye patch dispersion can be analysed on the basis of the recalculated tracks.

With the help of a statistical analysis the lateral eddy diffusivity coefficients were estimated from the depth integrated maps of dye distribution obtained for each survey according to the methodology of Ledwell et al. (1998). Observed values in the Celtic Sea study under investigation here were found to be in a range between 4.0 m^2 s^{-1} for surveys R2S1 and R2S2 to 1.9 m^2 s^{-1} for surveys R2S3 and R2S4 (Inall et al., 2013). The reasons for such temporal variability is discussed in Section "Influence of the shear currents".

Equivalent estimations of the effective diffusion for the dye patch can be done on the basis of the results of the numerical modelling. Agreement between the model and the field estimations of "effective" diffusivity values can be used as some kind of the proof of the validity of the model results on the evolution of the dye patch.

The dye dispersion in numerical model is controlled by three different processes: numerical diffusion, physical diffusion, and influence of the shear currents.

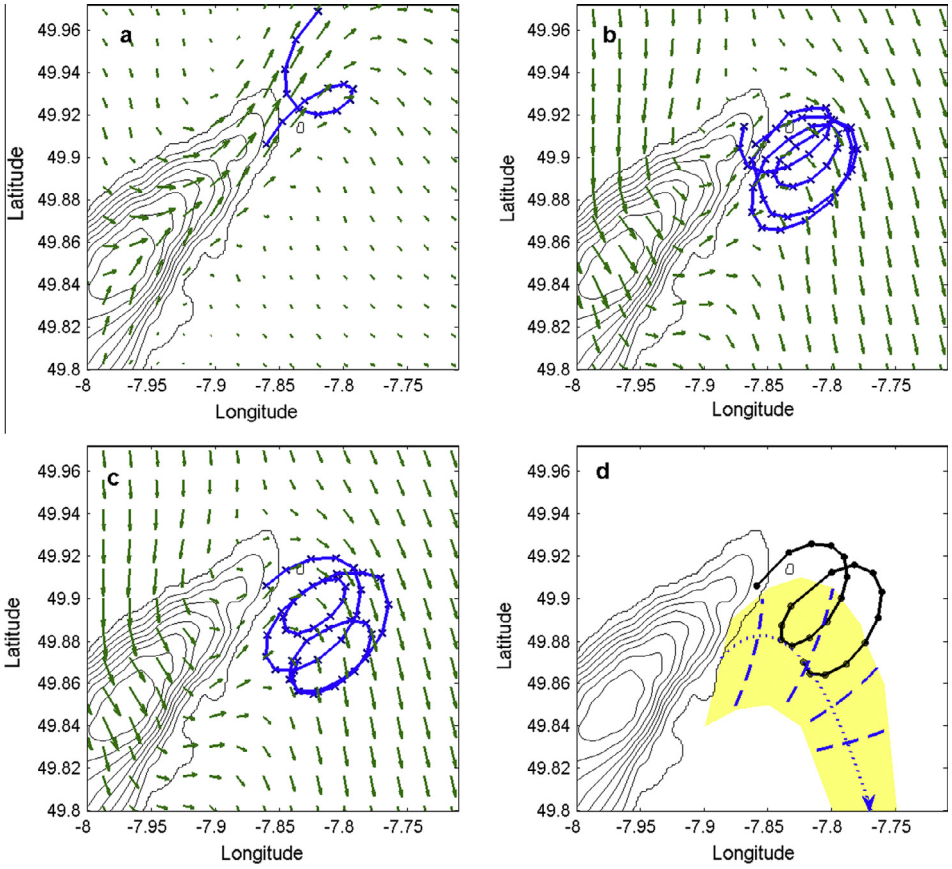

Fig. 5. 48-h Tracks of the model drifter when different forcing were activated in the model: (a) only tides, (b) tides and current and (c) tides, current and wind stresses. Arrows show the direction of the residual currents. (d) Track of the field drifter (24 h). Dashed lines show the fronts of internal waves generated by tides and radiated from Jones Bank. Yellow colour shows the area of intensive internal wave activity. Time interval between to fronts equals one hour (for the details see (Vlasenko et al., 2013)). (For interpretation of the references to colour in this figure legend, the reader is referred to the web version of this article.)

Numerical diffusion

The numerical diffusion is introduced by inaccurate numerical implementation of the governing equations and can be estimated by comparing model results with analytical solutions. An idealized vertically oriented cylindrical volume with the dye spreading horizontally due to diffusion with the coefficient D was used as a test bed. To achieve the best fit of analytical solution with the numerical profiles different values of D were used in the formula (A.5) for the analytical solution presented in the Appendix.

In the numerical experiment the dye spot was released as a vertical column of homogeneous fluid in a basin of constant depth. To estimate the contribution of the numerical diffusion that appears because of an inaccurate numerical implementation of the advection terms uC_x and vC_y in (1) the tidal current with velocities $u = v = 0.3$ m s^{-1}, typical for the Celtic Sea shelf, were added to the model. The value of the diffusivity coefficient K_h in MITgcm was taken to be identically zero, whereas the value of D in the analytical model was chosen in such a way as to find the best fit of the analytical solution to numerical solution.

Fig. 6a shows thirteen dye patches overlaid in one figure at a depth of 35 m for one tidal cycle with 50 min interval. It is seen that the dye that initially occupied only one numerical cell gradually spread into number of neighbouring cells due to the effects of numerical diffusion. The dye concentration in the numerical patch centre was taken as the reference value to estimate the value of the diffusion coefficient D. Both the numerically obtained and analytical distributions of the tracer concentration coincided, Fig. 6b, when the diffusion coefficient $D = 0.2$ m^2 s^{-1} was set in analytical model.

Physical diffusion

The second process that contributes to the dye dispersion is physical diffusion itself which develops due to subgrid scale mixing processes. In the next experiment the background model diffusivity K_h in the MITgcm was set to a value of 0.5 m^2 s^{-1}. In this case both numerical and (sub grid) physical diffusion act on the dye released in a vertical column of homogeneous fluid in the basin of constant depth with tides. Similar to Figs. 6a, 6c shows thirteen overlaid dye patches obtained for one tidal cycle at the depth of 35 m. The comparison of Fig. 6a and c reveals a more diffuse structure of the dye patches now. The estimation of the diffusion coefficient using the analytical solution gives a value 0.5 m^2 s^{-1}, Fig. 6d. Surprisingly, the numerical diffusion (earlier estimated at 0.2 m^2 s^{-1}) being smaller than the physical diffusion seems to be suppressed by the latter.

Influence of the shear currents

The third important physical process that can contribute to the dye dispersion is the vertical shear of background currents in the presence of vertical mixing. The estimation of dispersion is now based on an analysis of dye evolution during each of the four Scanfish survey. Fig. 7 represents six successive contours of the dye patch taken at one hour time intervals overlaid with the ship's

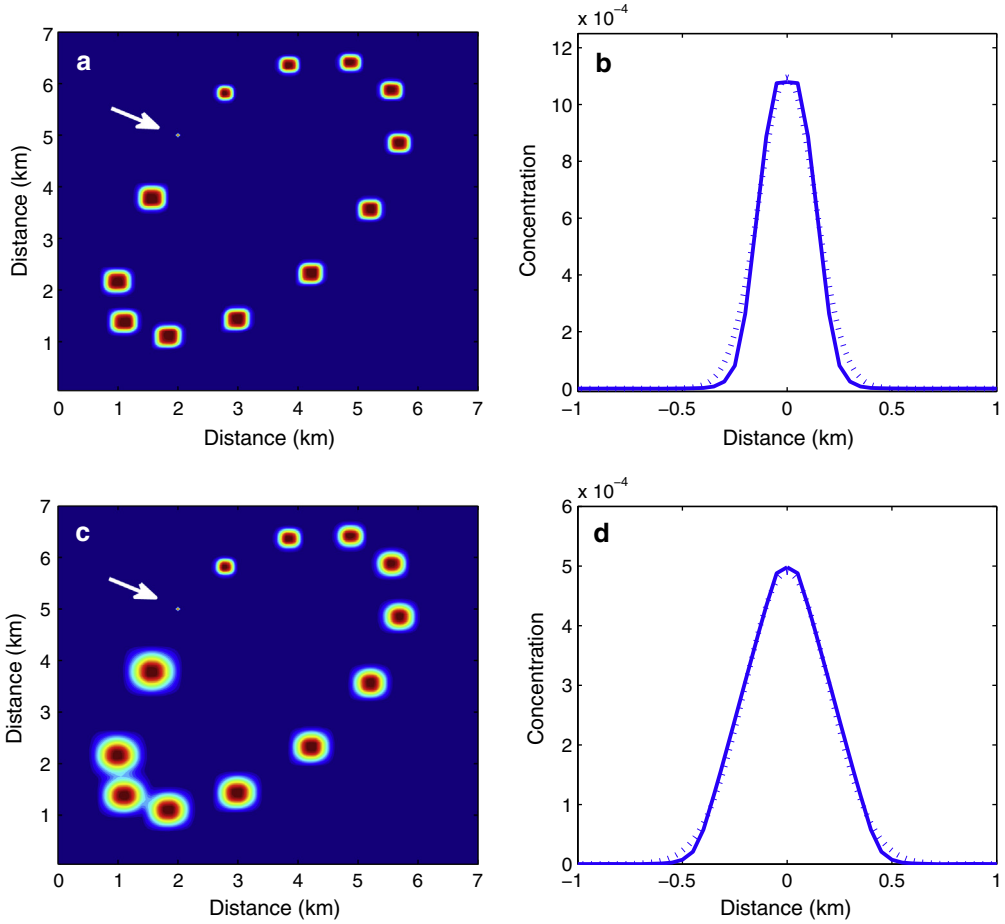

Fig. 6. Model predicted dye patches for one tidal cycle overlaid in one figure obtained when (a) $K_h = 0\ m^2\ s^{-1}$ and (c) $K_h = 0.5\ m^2\ s^{-1}$. Arrows show the position of initial dye spot. Dye distribution through the centre of the patch obtained for (b) model prediction with $K_h = 0\ m^2\ s^{-1}$ and analytical solution with $D = 0.2\ m\ s^{-2}$ and for (d) model prediction with $K_h = 0.5\ m^2\ s^{-1}$ and analytical solution with $D = 0.5\ m^2\ s^{-1}$. Model and analytical distributions are shown by solid and dashed lines, respectively.

track for surveys R2S1 (started 5 h and finished 10 h after the Rhodamine release, left top panel), and R2S2 (started 14 h and finished 20 h after the beginning of the dye release experiment, right top panel), Fig. 8 shows similar distributions but for survey R2S3 (started 27 h and finished 33 h after Rhodamine release) and R2S4 (started 39 h and finished 45 h after Rhodamine release). The dye concentration in both figures is taken at a depth of 35 metres. The three-dimensional distributions of the dye patch (slices at different depths) at the end of every survey are given in the lower panels of Figs. 7 and 8.

Analysis of Figs. 7 and 8 shows that the spatial structure of the dye patch is quite stable during each survey over the whole period of the dye release experiment. Note that the dye diffuses upward and downward from its initial position, 35 m depth, unevenly. At 25 m depth the dye concentration exceeds the similar value at 45 m depth, which suggests stronger upward dye fluxes.

Due to a velocity shear the dye patch stretches in horizontal directions quite differently at different depths. In combination with vertical diapycnal mixing this stretching results in a substantial increase of the "effective" horizontal dispersion of the dye patch. The "effective" diffusivity in this case was estimated in (Young et al., 1982) by the following formula:

$$K_e = K_h + \frac{1}{2}\left(\frac{\alpha}{\omega}\right)^2 K_z. \qquad (2)$$

Here α is the amplitude of velocity shear du/dz; ω is the frequency of the oscillating current; K_h is the coefficient of the background horizontal diffusivity, and K_z is the appropriate value of the vertical diffusivity.

In formula (2) ω is assumed to be the frequency of a dominant process that mostly contributes to the velocity shear. The power density spectra that were calculated at different depths using the model output for the position of mooring MS1, Fig. 9a, show that both inertial and semi-diurnal oscillations contributed to the amplitude of velocity shear α. Harmonic analysis of the velocities conducted for these dominant frequencies, Fig. 9b and c, revealed that semi-diurnal oscillations dominated the whole water column and were nearly in phase from the surface to bottom. At the same time the inertial oscillations attenuated dramatically with depth. A factor of two reduction in the current speed from the surface to the bottom with a substantial phase shift below the thermocline was reproduced by the model, similar to the field data (Inall et al., 2013).

The last variable that is still unknown in (2) is the amplitude of the vertical shear of the oscillating current α. This value was calculated using the difference in the positions of the dye patch at different depths at the start and the end of each survey divided by the time and depth steps. The "effective" diffusivity coefficients calculated for each survey were then found as follows: $K_e = 4.39\ m^2\ s^{-1}$ (R2S1), $K_e = 1.44\ m^2\ s^{-1}$ (R2S2), $K_e = 0.8053\ m^2\ s^{-1}$ (R2S3), and $K_e = 3.68\ m^2\ s^{-1}$ (R2S4). The values so obtained are in good agreement with those based on the in-situ observations (Inall et al., 2013).

A fivefold temporal variability of the diffusion coefficient K_e within 40 h deserves some further discussion. According to Fig. 9,

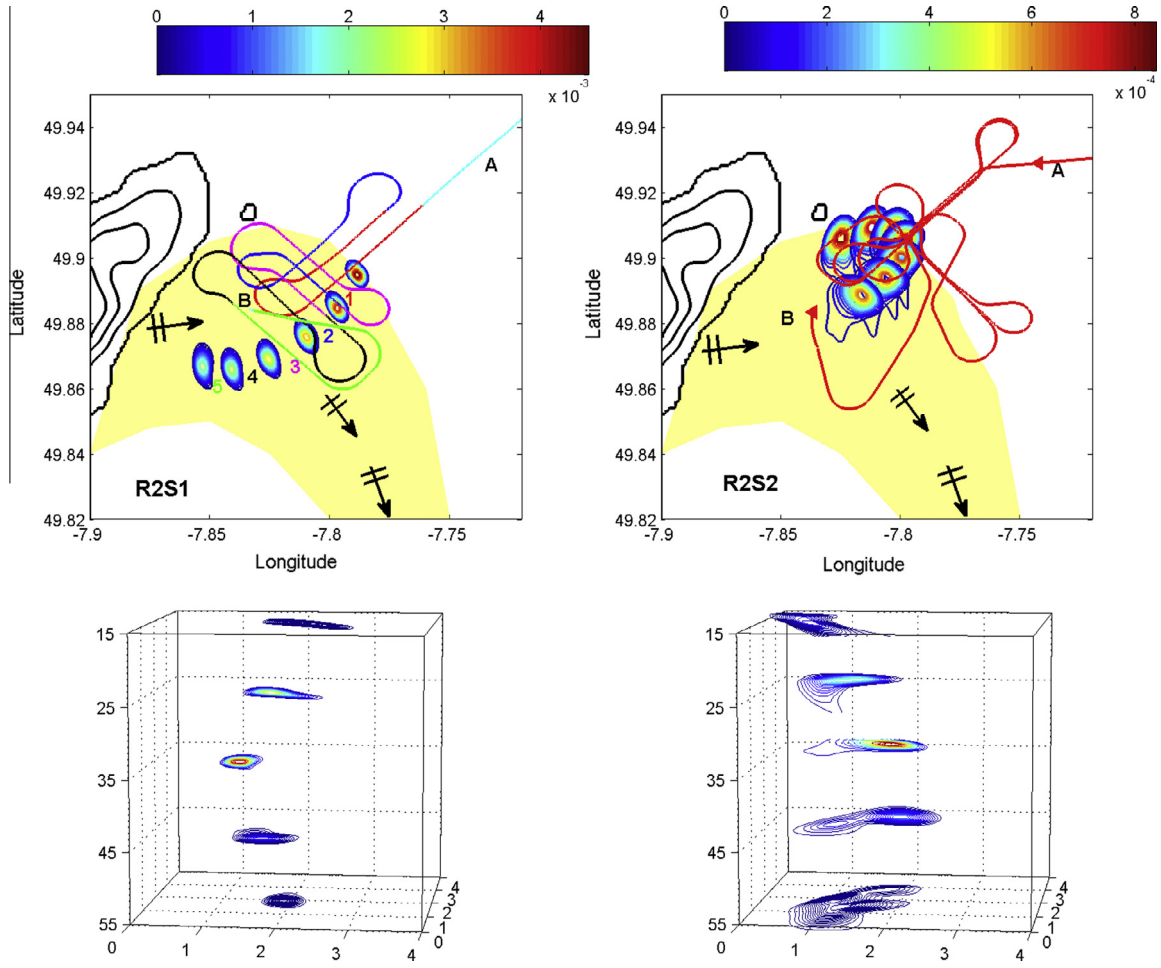

Fig. 7. (Top panels) Six successive contours of the model tracer taken with one hour time interval at the depth of 35 m overlaid with the Scanfish tracks for surveys R2S1 and R2S2. Letters A and B show the beginning and the end of each survey, respectively. (Bottom panels) Horizontal distribution of the tracer at different depths taken in the end of R2S1 (left panel) and R2S2 (right panel) surveys. Yellow zone with arrows shows the area and direction of propagation of the strongest internal wave systems generated by tides and presented in Fig. 5d (see also (Vlasenko et al., 2013)). Relative position of the ship and the dye patch during the survey R2S1 is shown by the same colour of the numbers between two successive positions of the patch and corresponding fragment of the ship track. (For interpretation of the references to colour in this figure legend, the reader is referred to the web version of this article.)

the inertial oscillations contribute to the effective diapicnal mixing. However, tidally generated internal waves are still missing from this analysis. The oscillations of internal waves in the area of Jones Bank can reach 40 m in vertical extent (Vlasenko et al., 2013), which is significant in comparison to the total water depth of 120 m. Such waves appear twice per day and have the structure of the first baroclinic mode with strong vertical shear which is a prerequisite for intensification of the effective horizontal dispersion.

Internal waves that are generated over the north-eastern flank propagated towards the dye release area. The waves route and wave front signatures are schematically shown in Fig. 5d (the yellow area corresponds to Wave 3 shown in Figure 6 of Vlasenko et al. (2013)). It is clear that the intensity of horizontal dispersion of the dye patch depends on whether the wave trajectory intersects with the dye patch trajectory or not. Taking into account that tidal excursion of the dye patch was 5–6 km and the wave propagation band is of the same order (approximately 5–10 km), one can assume that at some stages of the dye release experiment the patch may cross the pathway of the radiated waves, increasing the effective dye dispersion.

Comparing the intersected areas of the model dye patch and internal wave in Figs. 7 and 8 during the surveys R2S1–R2S4, one finds a highly plausible physical explanation for the temporal variability of the diffusion coefficient K_e. Survey R2S1 was entirely located in the area affected by the internal waves (Fig. 7) which is why the diffusion coefficient is maximal, $K_e = 4.39\ m^2\ s^{-1}$. Survey R2S2 was partly beyond the wave-yellow zone in Fig. 7, so the dye patch was less affected by internal waves and the dye dispersion was weaker, $K_e = 1.44\ m^2\ s^{-1}$. Fig. 8 shows that at least a half of the survey R2S3 was beyond the area affected by internal waves. As a result the dye dispersion is at the minimum level, $K_e = 0.8053\ m^2\ s^{-1}$. Finally, during the survey R2S4 the dye patch returned to the area affected by waves (Fig. 8), and as a result the dispersion increased, $K_e = 3.68\ m^2\ s^{-1}$.

Modelling of dye evolution for Scanfish surveys

The comparison of the modelled dye evolution and field data for all four Scanfish surveys, R2S1, R2S2, R2S3 and R2S4 will be based on the results presented in Figs. 10–13. Each of these figures shows the position and the time where and when the Rhodamine patch was recorded in-situ (every independent event is denoted by filled circles with unique colours). It should be noted that the towed undulated fluorometer was able to measure Rhodamine concentration continuously as a function of depth throughout the water column. Thus, we use the depth integrated dye concentrations on each profile to show model predicted contours of the

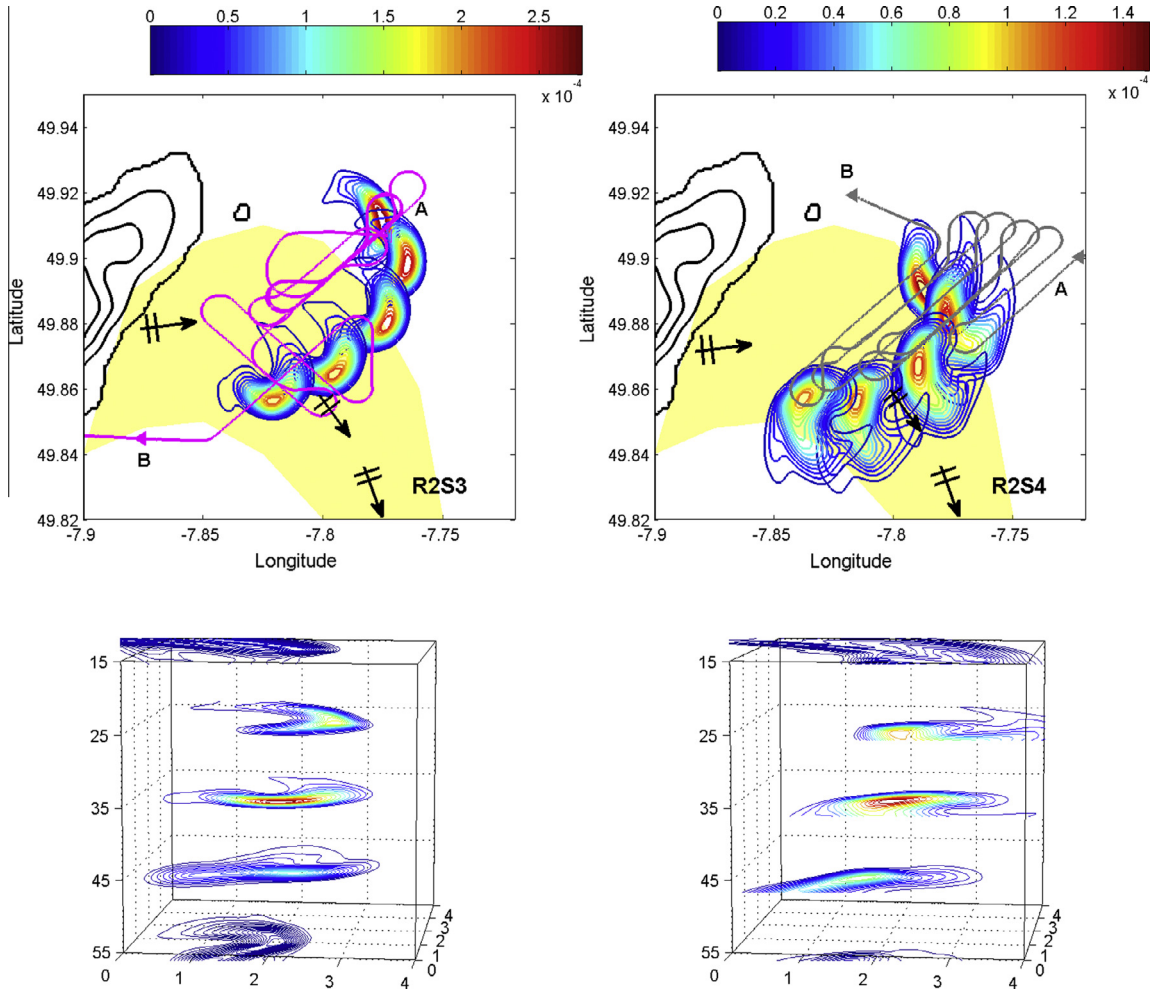

Fig. 8. The same as Fig. 7 but for surveys R2S3 and R2S4.

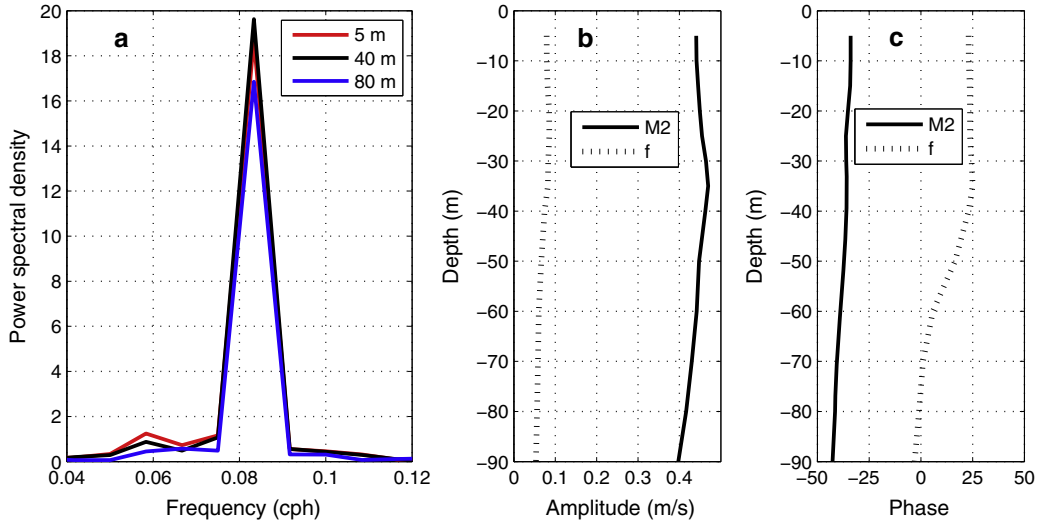

Fig. 9. (a) Model predicted velocity power spectra calculated for the position of mooring MS1. (b) Amplitude and (c) phase of inertial (dotted lines) and semi-diurnal (solid lines) currents as functions of depth.

dye patch along with the positions where the Rhodamine was detected by the Scanfish.

During the first Scanfish survey, R2S1, the fluorometer detected the dye patch only once (that is, on one profile). This event happened on $t = 199.3523$ Julian day (jday afterwards), i.e. on 17 July 2008 at 08:27, Fig. 10a, and the dye concentration was equal to 12 μg/l. The position where the Rhodamine was found is shown by a red filled circle on the map with ship's track. The arrow shows

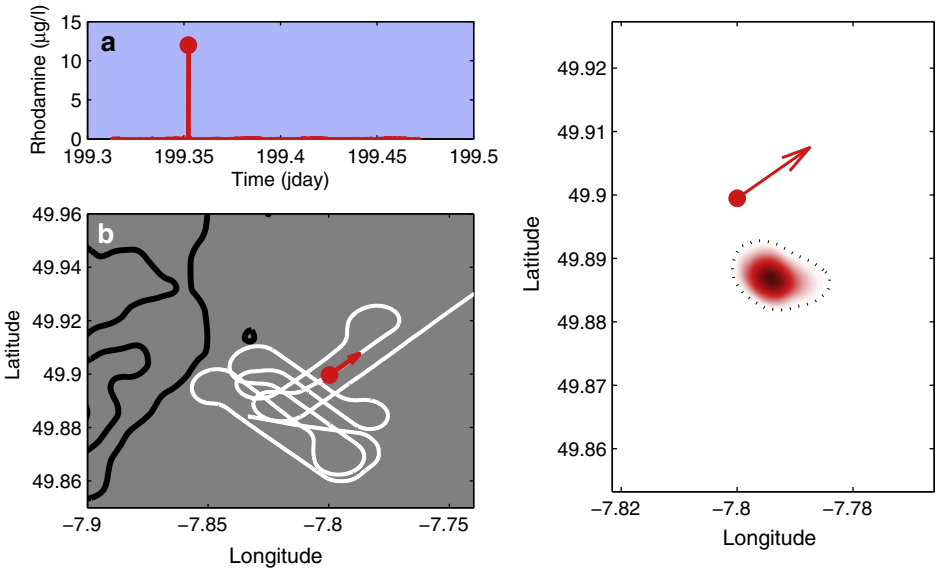

Fig. 10. (a) Time series of the Rhodamine concentration recorded in-situ by the Scanfish fluorometer during R2S1 survey. The ship tracks is shown by a white solid line in panel (b). The filled red circle in panel (a) shows the largest value that was recorded when the ship was at the position shown in panel (b) by the similar colour. The right panel shows the model predicted distribution of the tracer at the moment of time when the Rhodamine spike was recorded. Red arrow shows the position and the direction of the vessel. The outer contour marked by black line corresponds to the largest tracer concentration divided by 100. (For interpretation of the references to colour in this figure legend, the reader is referred to the web version of this article.)

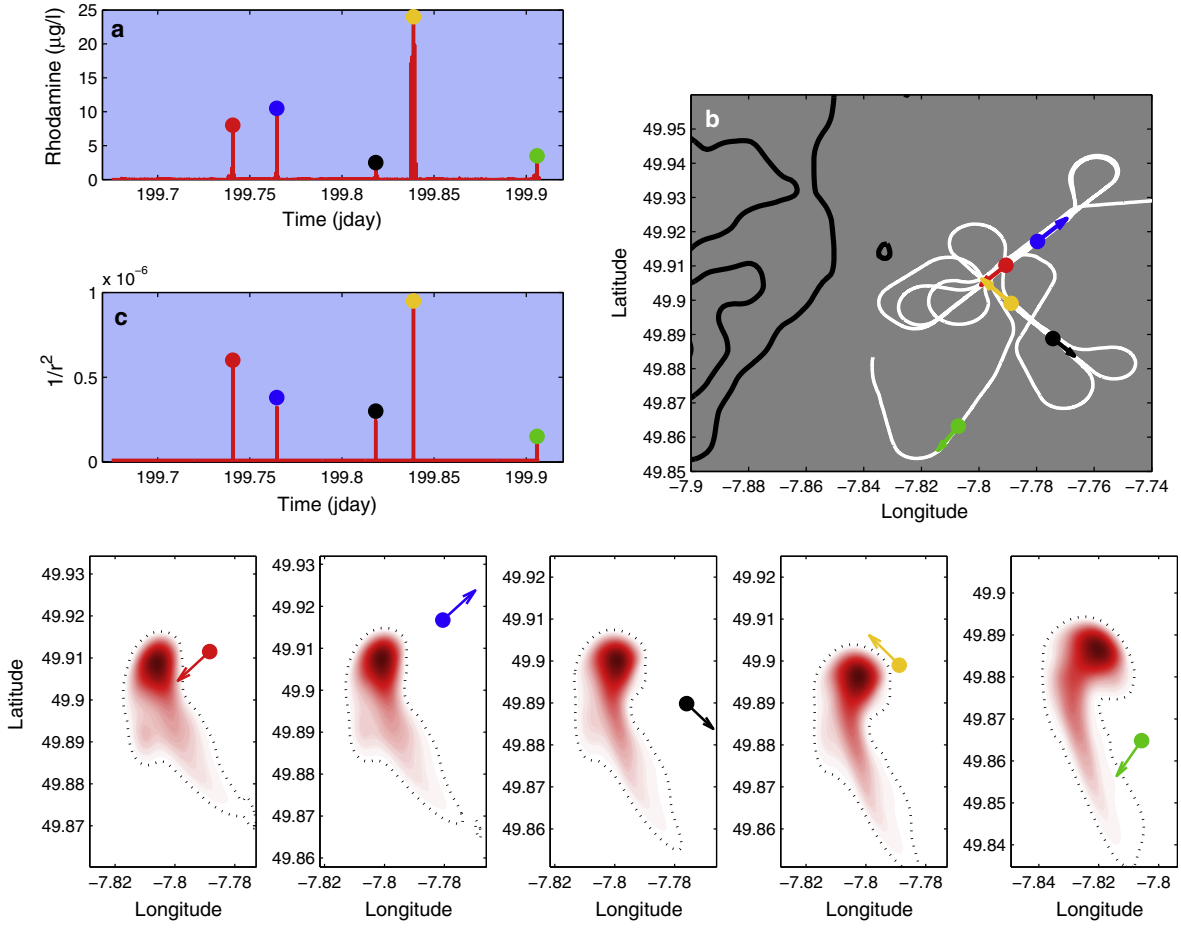

Fig. 11. (a) The time series of the Rhodamine concentration recorded in the field experiment during the survey R2S2. Red, blue, black, yellow and green filled circles on the top of each peack correspond to the position of the vessel (depicted by the similar colours in panel (b)) where these peacks were detected. (c) Model predicted time series showing the inverse square distance $1/r^2$ between the centre of the model tracer patch and an actual position of the vessel (see bottom panel) when the largest value of the Rhodamine was recorded in-situ. (For interpretation of the references to colour in this figure legend, the reader is referred to the web version of this article.)

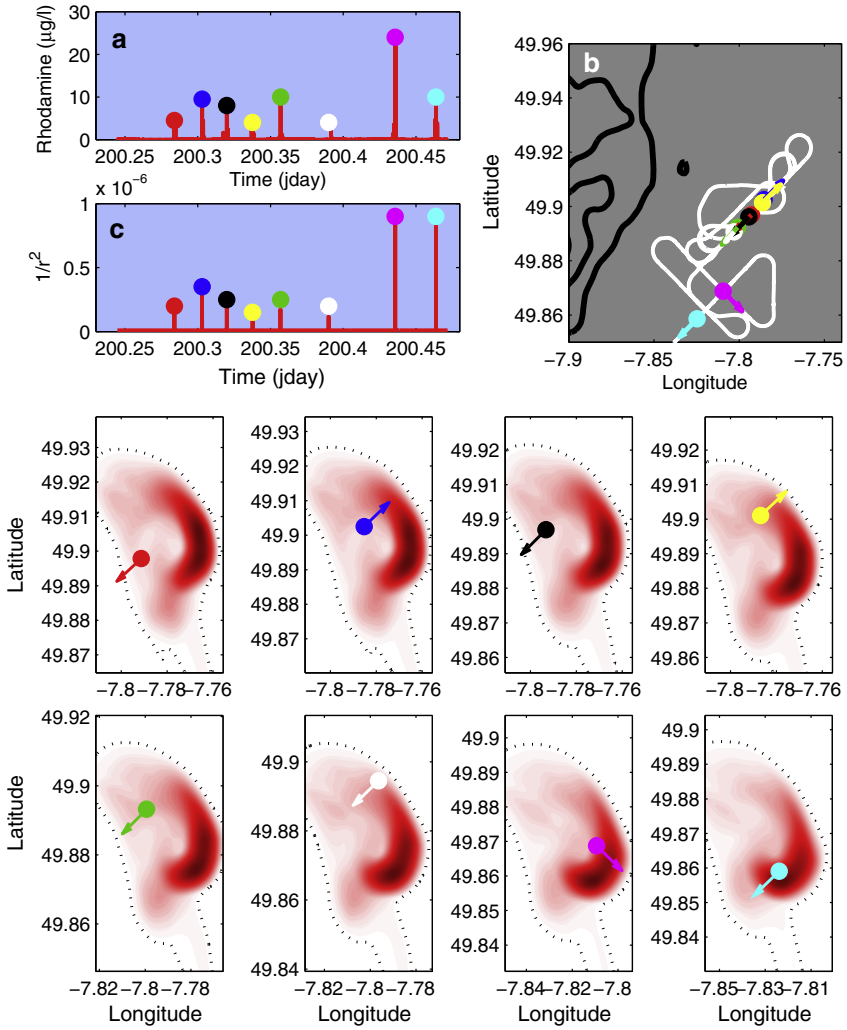

Fig. 12. The same as Fig. 11 but for the survey R2S3.

the direction of the vessel at that time. Taking into account that the value of the Rhodamine concentration was the smallest in comparison with the concentration detected during the next surveys (Fig. 2), it is clear that the dye cloud (that had just been released) must have been crossed by the vessel not exactly through its centre, where the concentration must have been considerably higher. The distance between model dye centre and filled red circle is 0.5 km.

Looking at the Scanfish survey, R2S1, and the evolution of the model dye patch shown in Fig. 7 it might be assumed (incorrectly) that the ship crossed the cloud of the dye several times, whereas Fig. 10 reveals only one spike of concentration. In fact, there is no contradiction between the two figures. Comparing the mutual positions of the colour fragments of the ship track shown in Fig. 7 with matching coloured numbers that show the trajectory of the patch at the very same time interval one can conclude the virtual vessel only once approached the model dye patch. Red colour provides the shortest distance between the ship and the dye patch. For the rest of the survey the (virtual) fluorometer was too far from the model Rhodamine cloud to detect it.

During the next Scanfish survey, R2S2, the fluorometer detected local maxima of the Rhodamine concentration that exceed the background value on five independent profiles, Fig. 11a. The measurements were between $t = 199.7408$ and 199.9059 jdays (from 17:46 to 21:42 on 17 July 2008). The red, blue, black, yellow and green filled circles are used here to associate corresponding peaks with their locations, Fig. 11b. Again, the arrows show the direction of the vessel at the time the dye was detected. It is clear that the intensity of local maxima are distributed randomly with time and can give only limited information on spatial configuration of the dye at this time. A deeper insight into the patch distribution can be revealed using some model results. Five bottom panels in Fig. 11 show the dye patch structure predicted by the model, i.e. how they are predicted to be at the five specific moments of the survey when dye was actually detected. Red, blue, black, yellow and green filled circles show the actual positions of the Scanfish when the evolving Rhodamine patch was recorded in-situ. All bottom panels are shown to the same scale, i.e. in a rectangle with 8 km size in meridional and 4 km in zonal directions.

Taking into account the number of assumptions necessary in the model set-up, it is not clear in advance that the model prediction would be of sufficient quality to aid our interpretation of the observed dye distribution. In a very general case the modelled dye evolves initially isotropically in all directions creating circular contours with equal concentrations that are proportional to the inverse squared distance from the centre of the cloud. It is suggested therefore to use here the inverse squared distance r^{-2} between the blue, black, yellow and green circles and the corresponding centre of the model patch from the bottom panels of Fig. 11 as a measure of model's skill in predicting the dye distribution. Fig. 11c shows the inverse squared distances r^{-2} as function of time, where all peaks are accompanied by corresponded coloured

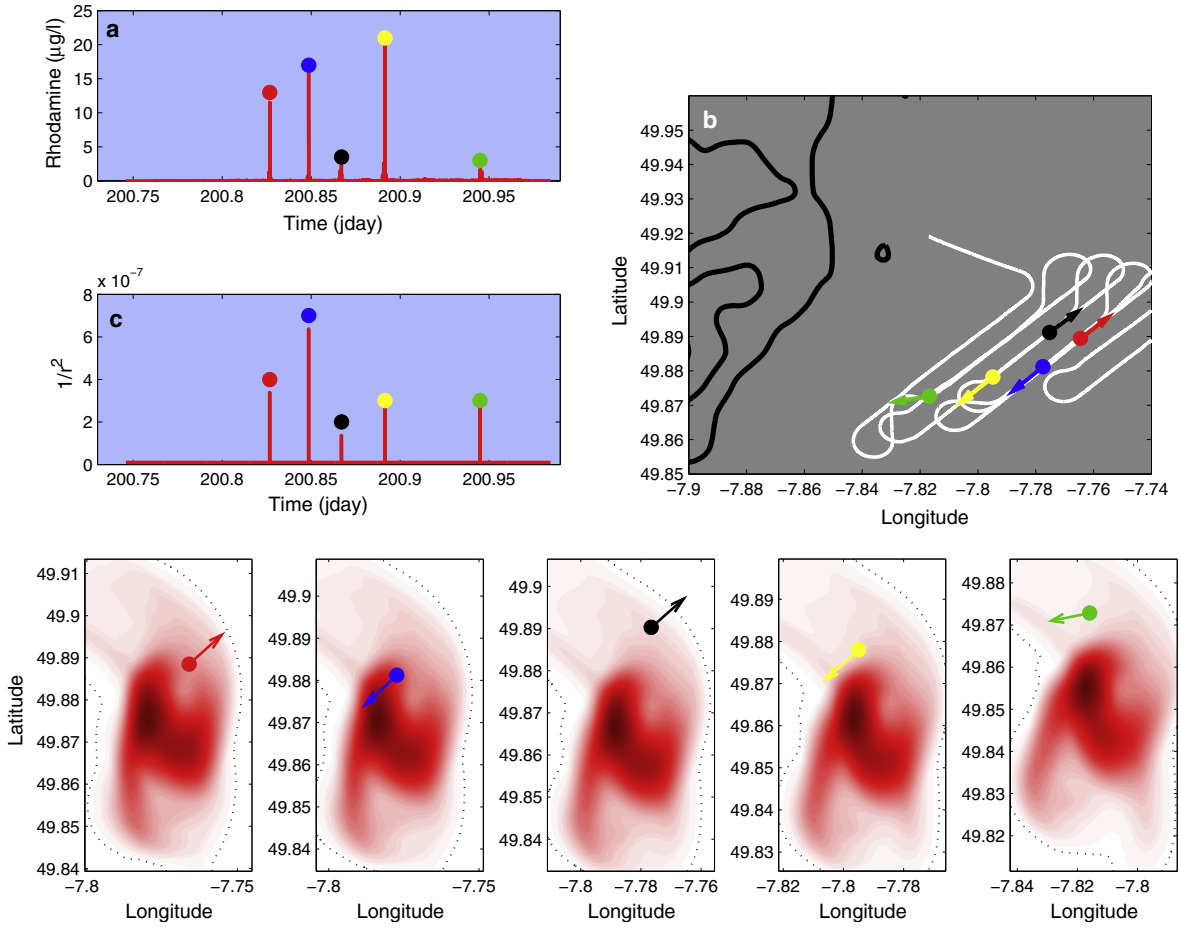

Fig. 13. The same as Fig. 11 but for the survey R2S4.

filled circle. Comparison of peaks of field dye concentration, Fig. 11a and the peaks of squared inverse distances, Fig. 11c shows a very good correlation.

Eight independent local maxima of the Rhodamine concentration were detected during the third Scanfish survey, R2S3, Fig. 12. The coloured filled circles in Fig. 12a and b show the time and the positions of the vessel with directions when they were captured by the fluorometer. Eight corresponding model predicted dye contour maps are shown in the bottom panels for domains with 8 km × 4 km and are overlaid with the circle of the corresponding colour. The time series of inverse squared distances r^{-2} between the position of the vessel marked by coloured circles and the maximum of model predicted dye patch is shown in Fig. 12c. It is seen that the vast majority of the peaks in Fig. 12c are in a very good agreement with the peaks shown in Fig. 12a. There is one clear exception (cyan, closest to the dye centre). The peak with a cyan circle is twice as large as the corresponding experimental data in Fig. 12c. However, this position is close to the strongest spatial gradients in the modelled dye concentration (and by inference also the real dye gradients), therefore even small uncertainties in the exact position of the observations (that is, the precise position of the Scanfish vehicle behind the vessel) could account for this discrepancy. Overall the correlation found between theoretical (modelled) and experimental can legitimately be classified as excellent.

During the final Scanfish survey, R2S4, five local maxima of the dye concentration were detected, see Fig. 13a and b. By now the model predicted patch filled the whole 8 km × 4 km domain and its contours do not present any symmetric configuration. However, the correlation between the experimentally recorded maxima, Fig. 12a, and inverse squared distance r^{-2}, Fig. 13c once again is very good with exception for the "yellow" peak.

Discussion and conclusions

Human exploitation of the oceanic shelf seas for food production, energy or chemicals, for tourism and gas/oil industry puts great stress on the shelf seas marine environment. All near-shore activities contain the potential risk that the sea could be polluted by some harmful substances. Being released into sea waters all dissolved or suspended materials disperse from the centre of contamination due to prevailing currents, their gradients and the associated irreversible turbulent mixing. Thus, an accurate method for the prediction of this spreading is a task with high priority for coastal zone management.

In general, there are two principal methods for estimating horizontal diffusivity in-situ. The first one is based on the analysis of the current meter data. In this method the horizontal diffusivity coefficients are calculated using turbulent velocity pulsations (Reynolds decomposition). An alternative and more direct method relies on the distribution of tracer data collected during dye release experiments.

Rhodamine dyes are normally preferred for tracer experiments compared with other chemicals or radioisotopes because of (a) their remarkable detectability, especially Rhodamine WT (concentrations smaller than 0.03 µg/kg may be detected by modern fluorometers), and (b) because of the relative simplicity of the

fluorometric measuring procedures. One such experiment with the Rhodamine WT was conducted from on board the R/V "*James Cook*" near Jones Bank in the Celtic Sea in July 2008 (Inall et al., 2013). The dye was injected into the pycnocline at a depth of approximately 35 m (approximately the level of the buoyancy frequency maximum), which was roughly 80 metres above the bottom. Scanfish, a towed undulating device connected by a cable to the vessel, was used in its undulation mode for an operational spatio/temporal survey of the thermohaline structure. Scanfish was also equipped with a fluorometer sensor which allowed for Rhodamine detection. Based on these in-situ collected data, the dye patch dispersion was quantified and reported elsewhere (Inall et al., 2013).

Isopycnal diffusion is a combination of two factors that normally contribute to the dye dispersion within a stratified fluid. The first one is an ordinary turbulence mechanism which is usually parametrized by second derivatives of the concentration (Fick's law of diffusion). The second mechanism concerns the horizontal mixing induced by shear currents (so-called "shear dispersion" first described by G.I. Taylor in 1953). The possibility of such a mechanism was pointed out by Young et al. (1982) who assumed that shear currents in combination with vertical diapycnal mixing can lead to an increase of the "effective" horizontal dispersion of the dye patch. One of the primary targets of the dye release experiment conducted in the Celtic Sea shelf in July, 2008 and discussed in (Inall et al., 2013) was to specify the role which shear currents can play in enhancement of the isopycnal mixing, and to identify the dominant forcing mechanism of the shear currents. The estimated effective values of the horizontal diffusion coefficients at different stages of the 2-day field experiment varied from 1.9 to 4 $m^2\ s^{-1}$.

The present paper was motivated by the intention to test the idea that a fine resolution numerical model could replicate the dye release experiment with sufficient accuracy so that it could be used to "fill up" all the gaps in the dye patch surveys, and be able to come out with quantitative estimates of the mixing coefficients that are, at least, consistent with the observations. If this were to be the case, then it would represent a great progressive step in the planning of observational campaigns of dye release experiments, and significantly aid the further analysis and interpretation of the in-situ data. The ability of models to reproduce dispersion under realistic conditions (shear currents, wind, tides) over several days is a sensitive criterion for evaluating the degree of their reliability.

A very promising outcome from the numerical experiments reported here is the very good correlation between the experimentally detected dye concentrations and their model predicted counterparts. Bearing in mind that in-situ data collected on the dye patch distribution in the field experiment assume a level of spatial uncertainty, the good coincidence with the model allows us conclude that an accurate application of numerical models of the type used here has a great potential for estimations of the water mixing in general, and in dye release experiments in particular.

It should be noted here that the presented model approach is not the only possible way to aid the sparse sampling. An alternative methodology for the prediction of the transport of dye or biological forms can be based on data assimilative hindcast, as reported by (Aretxabaleta et al., 2005). This method starts with a forward model Quoddy (Lynch et al., 1996) as a prior estimate. Comparison of the obtained solution with the observational data gives the difference between the observations and model estimates at the data locations, called the "misfit". The estimates of misfit provided by this special procedure is described in Lynch and Hannah (2001), Lynch and Naimie (2002). Then the data assimilation procedure to the barotropic boundary conditions is used for large values of misfit. The misfit is recomputed and the procedure is continued until convergence is found. Being quite quick in replication of the velocity and dye fields in desired area, such an approach however requires a series of ADCP measurements in the same domain, which is not always possible. In fact, the combination of the two can give the best result.

Acknowledgement

This work was initiated during the start of Natural Environment Research Council (UK), Grant FASTNEt NE/I030224/1.

Analytical solution of a diffusion problem in cylindrical coordinates

Consider an infinite cylindrical domain of radius R filled with water. Centrally located internal co-axial cylindrical volume of water with the radius r_0 contains some dye with initial concentration C_0. The evolution of the dye concentration C is described by the following initial value problem:

$$\frac{\partial C(r,t)}{\partial t} = D\frac{1}{r}\frac{\partial}{\partial r}\left(r\frac{\partial C(r,t)}{\partial r}\right), \tag{A.1}$$

$$C(r,0) = \begin{cases} C_0, & r \leqslant r_0, \\ 0, & r > r_0, \end{cases} \tag{A.2}$$

$$C(R,t) = 0. \tag{A.3}$$

Assuming that the solution of problem (A.1)–(A.3) can be presented in terms of two independent functions $P(r)$ and $T(t)$ as follows $C(r,t) = P(r)T(t)$ the method of separation of the variables leads to two independent equations for these functions P and T:

$$\frac{dT}{dt} = -\lambda^2 DT, \quad \rightarrow \quad T(t) = A\exp(-\lambda^2 Dt);$$

$$\frac{d}{dr}\left(r\frac{dP}{dr}\right) + \lambda^2 rP = 0, \quad \rightarrow \quad P(r) = BJ_0(\lambda r) + EY_0(\lambda r).$$

Here A, B, and E are unknown coefficients, λ is some constant value, J_0 and Y_0 are the Bessel function of the first and the second kind, respectively. It is clear that $E = 0$ because the function $P(r)$ should be finite at $r \to 0$. If so the solution of (A.1)–(A.3) reads:

$$C(r,t) = AJ_0(\lambda r)\exp(-\lambda^2 Dt). \tag{A.4}$$

Two unknown values, i.e. A and λ, can be found using boundary conditions. It is clear that the boundary condition (A.3) is valid only if $J_0(\lambda R) = 0$. The function $J_0(\alpha_m)$ $(m = 1, 2, 3, \ldots)$ has an infinitive number of real zeros at $\lambda_m R = \alpha_m$. If so the analytical solution (A.4) reads:

$$C(r,t) = \sum_{m=1}^{\infty} A_m \exp(-\lambda_m^2 Dt) J_0(\lambda_m r). \tag{A.5}$$

Initial condition (A.2) is used to find A_m:

$$\sum_{m=1}^{\infty} A_m J_0(\lambda_m r) = C_0.$$

Using the orthogonal property of the Bessel function, i.e.

$$\int_0^R J_0(\lambda_m r) J_0(\lambda_j r) r dr = \begin{cases} 0, & \text{if} \quad m \neq j, \\ \frac{R^2}{2} J_1^2(\lambda_m R), & \text{if} \quad m = j, \end{cases}$$

it is possible to find the amplitudes which are calculated as follows:

$$A_m = \frac{2C_0 \int_0^R J_0^2(\lambda_m r) r dr}{R^2 J_1^2(\lambda_m R)}.$$

References

Aretxabaleta, A., Manning, J., Werner, F.E., Smith, K., Blaton, B.O., Lynch, D.R., 2005. Data assimilative hindcast on the Southern Flank of Georges Bank during May 1999: frontal circulation and implications. Cont. Shelf Res. 25, 849–874.

Beckmann, A., 1995. Numerical modeling of the time-mean flow at isolated seamounts, 'Aha Huiliko'a Hawaiian Workshop 1995, pp. 57–66.

Egbert, G.D., Erofeeva, S.Y., 2002. Efficient inverse modeling of barotropic ocean tides. J. Atmos. Oceanic Technol. 19 (2), 183–204.

Huthnance, J.M., 1974. On the diurnal tidal currents over Rockall Bank. Deep Sea Res. Oceanogr. Abstr. 21 (1), 23–35.

Inall, M., Aleynik, D., Neil, C., 2013. Horizontal advection and dispersion in a stratified shelf sea: the role of inertial oscillations. Progr. Oceanogr. 117, 25–36.

Kowalik, Z., Marchenko, A.V., 2002. Tidal motion enhancement around islands. J. Mar. Res. 60, 551–581.

Ledwell, J.R., Watson, A.J., Law, C.S., 1998. Mixing of tracer in the pycnocline. J. Geophys. Res. 15, 21499–21529.

Ledwell, J.R., Duda, T.F., Sundermeyer, M.A., Seim, H.E., 2004. Mixing in coastal environment: 1. A view from dye dispersion. J. Geophys. Res. 109. http://dx.doi.org/10.1029/2003JC002194.

Loder, J.W., 1980. Topographic rectification of tidal currents on the sides of Georges Bank. J. Phys. Oceanogr. 10, 1399–1416.

Lynch, D.R., Hannah, C.G., 2001. Inverse model for limited-area hindcasts on the continental shelf. J. Atmos. Oceanic Tech. 18, 962–981.

Lynch, D.R., Naimie, C.E., 2002. Hindcasting the Georges Bank circulation, Part II: Wind-band inversion. Cont. Shelf Res. 22, 2191–2224.

Lynch, D.R., Ip, J.T.C., Naimie, C.E., Werner, F.E., 1996. Comprehensive coastal circulation model with application to the Gulf of Maine. Cont. Shelf Res. 16, 875–906.

Marshall, J., Adcroft, A., Hill, C., Perelman, L., Heisey, C., 1997. A finite-volume, incompressible Navier–Stokes model for studies of the ocean on the parallel computers. J. Geophys. Res. 102, 5733–5752.

Nash, J.D., Moum, J.N., 2001. Internal hydraulic flow on the continental shelf: high drag states over a small bank. J. Geophys. Res. 106 (C3), 4593–4611.

Pacanowski, R.C., Philander, S.G.H., 1981. Parameterisation of vertical mixing in numerical models of Tropical Oceans. J. Phys. Oceanogr. 11, 1443–1451.

Sundermeyer, M.A., Ledwell, J.R., 2001. Lateral dispersion over the continental shelf: analysis of dye release experiments. J. Geophys. Res.: Oceans 106, 9603–9621.

Vlasenko, V., Stashchuk, N., Palmer, M.R., Inall, M.E., 2013. Generation of baroclinic tides over an isolated underwater bank. J. Geophys. Res.: Oceans 118. http://dx.doi.org/10.1002/jgrc.20304.

Young, W.R., Rhines, P.B., Garrett, C.J.R., 1982. Shear-flow dispersion, internal waves and horizontal mixing in the ocean. J. Phys. Oceanogr. 12, 515–527.